Simulation of the propagation of an acoustic wave through a turbulent velocity field: A study of phase variance[a]

M. Karweit[b]
Department of Chemical Engineering, The Johns Hopkins University, Baltimore, Maryland 21218

Ph. Blanc-Benon, D. Juvé, and G. Comte-Bellot
Laboratoire de Mécanique des Fluides et d'Acoustique, C.N.R.S. UA 263, Ecole Centrale de Lyon, 69131 Ecully Cedex, France

A numerical technique for simulating the behavior of an acoustic wave propagating through a turbulent medium is introduced. The technique involves two elements: the generation of 3-D, random, hypothetical, isotropic velocity fields in terms of a collection of discrete Fourier velocity modes; and the integration of the ray-trace equations to describe the trajectories of points tagging an acoustic wave front. The propagation times for these points to travel fixed distances through each of an ensemble of random velocity fields are recorded, and the variance of travel time (or acoustic phase) over the ensemble is calculated. In numerical ray-trace experiments through fields having average perturbation indices ≈ 0.01, acoustic travel-time variances are obtained that have a higher-order dependence on travel distance R than the classical Chernov prediction—a linear increase with R. The Chernov result is obtained, however, when the rays are confined to axial trajectories. Additional numerical experiments integrating the stochastic Helmholtz equation and its parabolic approximation yield time-variance estimates consistent with the ray-trace results. Predictions from these simulations are then applied to the laboratory experiments of Blanc-Benon and found to be in qualitative agreement. Finally, a set of 2-D travel-time experiments are presented to identify differences between source–receiver eigenray propagation and preassigned initial direction ray propagation.

PACS numbers: 43.20.Wd, 43.20.Fn, 43.28.Py, 43.20.Dk

INTRODUCTION

One of the more interesting features of sound is that its propagation characteristics are greatly influenced by the medium through which it travels. Through the processes of convection, refraction, and scattering, acoustic waves may be bent, attenuated, or amplified, or, in fact, rendered completely incoherent. Since the coherence and integrity of acoustic waves play fundamental roles in harmonic sound transmission, noise control, and sonic detection schemes, an understanding of how an acoustic wave is affected by its medium of propagation is essential.

In particular, the dispersion of sound in the atmosphere and the ocean is of interest. Both of these media are characterized by random inhomogeneities in velocity and temperature over an entire spectrum of scales. But because these natural environments are not well controlled, investigating how sound may be influenced by them is better undertaken within the turbulent or thermal field producible by a grid or jet in the laboratory.

An important measure of the influence of random inhomogeneities is the variation of phase as acoustic waves propagate through the medium. Two approaches for studying this variance have thus far been taken: a purely mathematical one in which wave-or ray-propagation equations are simplified and averaged to account for the random environment; and a laboratory one in which sound-propagation fluctuations are actually measured and interpreted.

The classical mathematical treatments are Tatarski (1971) and Chernov (1960). More recently, this literature has been expanded by Ishimaru (1978), Tatarski and Zavorotnyi (1980), and Flatté (1983). Efforts focusing on the stochastic Helmholtz equation and its parabolic approximation are especially of interest. In these approaches, the interaction between turbulence and acoustics is expressed in terms of a random index related to the temperature or velocity fluctuations, e.g., Candel (1979). Solutions are then obtained by various techniques: path integrals—Dashen (1979) and Fishman and McCoy (1984); phase screen–Codona *et al.* (1985) and Uscinski (1985); two-scale asymptotic expansions—Whitman and Beran (1985).

Experimental approaches are found in Blanc-Benon (1981) (B-B) and Ho and Kovasznay (1974), with measurements of acoustic propagation in fluctuating velocity fields. Blanc-Benon *et al.* (1986) addresses the problem in fluctuating temperature fields.

In this paper we offer a third approach—explicit numerical simulation of the motion of an acoustic ray propagating through a hypothetical, inhomogeneous velocity field. The hypothetical field consists of a small number of randomly oriented, discrete, Fourier velocity wave vectors whose amplitudes have been chosen to produce a distribu-

---

tion of velocities comparable to those found in experimental flows, i.e., the grid-generated turbulent flow of Comte-Bellot and Corrsin (1971) (C-BC), and the jet-generated turbulent flow of B-B. Making the assumption of a "frozen" velocity field and a weak acoustic wave front that does not interact with the field, we use the ray-trace equations to integrate numerically the trajectories of acoustic rays. By carrying out such integrations over an ensemble of statistically similar velocity fields, we accumulate statistics of the variation in arrival times for the rays traveling prescribed distances.

In our approach two features are noteworthy. First, most of our numerical experiments do not model the usual source–receiver problem in which the properties of eigenrays passing from source to receiver are investigated. Rather, we explore the propagation statistics of rays whose initial directions are preassigned without regard to where they may travel. (Below, in a comparison experiment involving eigenray tracing we refer to these preassigned initial direction rays as PID rays.) Second, in our method there is no inherent acoustic wavelength. To interpret travel-time variance as phase variance, we must multiply by an assumed angular frequency.

The present paper describes a number of numerical experiments, all of which focus on the travel-time variance of an acoustic wave propagating through a random inhomogeneous medium (air). In these experiments, in part because of the way we characterize the turbulent fields, and in part because of our procedure for following individual rays, we have the flexibility of obtaining solutions to the ray-trace equations with or without simplifying assumptions. Of the set of experiments, three simulate theoretical approximations by integrating ray-trace equations that have been modified to conform to the simplifying assumptions made in the respective theories. The theories examined are as follows: the Chernov approximation—propagation in a straight line; the stochastic Helmholtz solution—replacing a vector disturbance field with an "equivalent" scalar one; and the parabolic approximation—a forward scattering approach.

Two additional experiments complete our work: a simulation that does emulate a source–receiver problem (in two dimensions), and a simulation that models the laboratory work of B-B. In this latter effort, we statistically reproduce B-B's jet-generated air flow and compare our ray-trace calculations with his results.

I. GENERATING THE TURBULENT FIELD

With an eventual goal of modeling the jet-generated turbulent field used in B-B's acoustic measurements, we first established that our Fourier-mode approach to simulating such fields was viable. We validated our technique by generating fields comparable to the grid-generated turbulence used and fully described by C-BC. Jet-generated flows 20 nozzle diameters downstream and grid-generated flows 40 grid-mesh lengths downstream are quasi-isotropic and in spectral equilibrium. As such, their spectral forms are expected to be similar; and their statistical properties should differ only by a length scale L_0 and a turbulence level $u_1' = \sqrt{\overline{u_1^2}}$, u_1 being the component of velocity fluctuation in the x_1 direction.

To generate fields for our simulations, we used an adaptation of the spectral model for incompressible, isotropic turbulence due to von Karman (see, for example, Hinze, 1959) in which the shape of the energy density $E(k)$ is characterized by a single length scale $L_0 = 1/k_0$. Specifically, $E(k) \sim k^4/(k^2 + 1/L_0^2)^{17/6}$; and a value $L_0 = 0.032$ m gave a reasonable fit to the C-BC data. However, this simple spectral form, in principle, has an undefined Taylor microscale because, for large k, velocity gradients increase indefinitely with k. Therefore, there is also no definable "inner scale" of the field. (In practice, an effective Taylor microscale would exist because our spectra are truncated at a prescribed maximum wave number.) Although the inner scale is relatively unimportant in acoustic phase variance (Tatarski 1971), we modified the simple von Karman spectrum to include a spectral "tail" due to Pao (1965, 1968); thus our final spectral form was $E(k) \sim k^4/(k^2 + 1/L_0^2)^{17/6} \exp(-2.25(\eta k)^{4/3})$, where η is the Kolmogorov microscale. (In the flow of C-BC, $\eta = 0.0001$ m. However, in our simulations we experimented with η's ranging from 0.000 to 0.005.) With this spectral form, we then generated simulated turbulent fields that were composed of $N = 30$ to $N = 60$ independent Fourier modes, each having a randomly oriented wave vector k and a complex amplitude vector $a(k)$.

The direction of k was prescribed by means of the orientation angles θ and φ. These were picked randomly with probability $P(\theta) = \sin \theta /2$ and $P(\varphi) = 1/2\pi$. This ensured statistical isotropy with respect to k. The direction of $a(k)$ was also chosen randomly, but in a plane perpendicular to k (a requirement for an incompressible field). Here, a single angle ψ, chosen with uniform probability over $-\pi < \psi < \pi$, prescribed that orientation. The amplitude of $a(k)$ was defined to be $\sim E(k)^{1/2}$ to produce the von Karman distribution of velocities; and the complex phase of $a(k)$ was chosen randomly. Figure 1 illustrates this spectral description of a Fourier velocity mode.
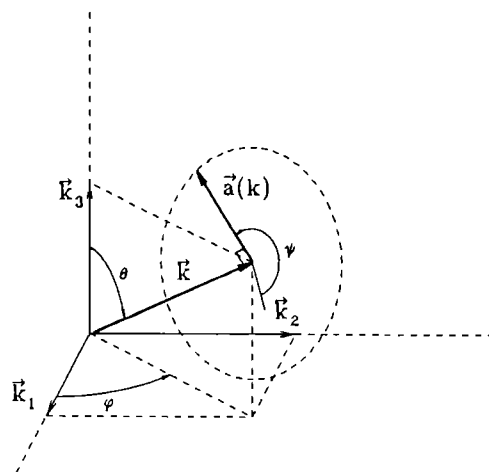
FIG. 1. Wave-vector geometry of a single Fourier velocity mode. For a given wave vector k with direction specified by θ and φ, a complex amplitude vector a(k) is produced as follows: a(k) lies in the plane perpendicular to k with arbitrary orientation ψ; the magnitude $|a(k)| \sim E(k)^{1/2}$; the complex phase is arbitrary (not shown).

To produce a purely real velocity field, for each randomly selected mode we included its conjugate counterpart with wave vector $-\mathbf{k}$ and conjugate amplitude vector $\mathbf{a}^*$. A complete velocity field was then defined as the summation of all these Fourier components, or

$$\mathbf{u}(\mathbf{x}) = \sum_{j=1}^{N} \mathbf{a}_j \exp(i\mathbf{k}_j \cdot \mathbf{x}) + \sum_{j=1}^{N} \mathbf{a}_j^* \exp(-i\mathbf{k}_j \cdot \mathbf{x}); \quad (1)$$

$\mathbf{a}$ was scaled to yield the desired rms velocity amplitude. Note also that this Fourier representation produces a field whose average velocity is zero, i.e., the field is a purely "fluctuating" field in space.

The collection of wave vectors that defined a field were chosen at logarithmic intervals between a minimum wave number $k = 1$ m^{-1} and a maximum wave number, usually $k = 1000$ m^{-1}. Figure 2 shows the spectral description of our simulated field using 30 modes and is superposed on the data of C-BC for comparison.

The principal decisions for constructing these velocity fields were four: How many Fourier modes need be used? Over what spectral range should the modes be defined? How should these modes be distributed within this range? Should the velocity-vector amplitudes be defined deterministically by the von Karman relationship, or should they be defined randomly with means corresponding to the von Karman relationship?

The decision on the number of modes was a practical one. Most of our numerical experiments were run with 30. In generating statistics for our simulation of acoustic propagation, the number of realizations times the number of Fourier modes representing the velocity field determined the computational time. Our disposition was to lean toward more realizations in lieu of more velocity modes. Trial experiments showed that increasing the number of independent modes to 60 did little to improve the stability of the statistics (except
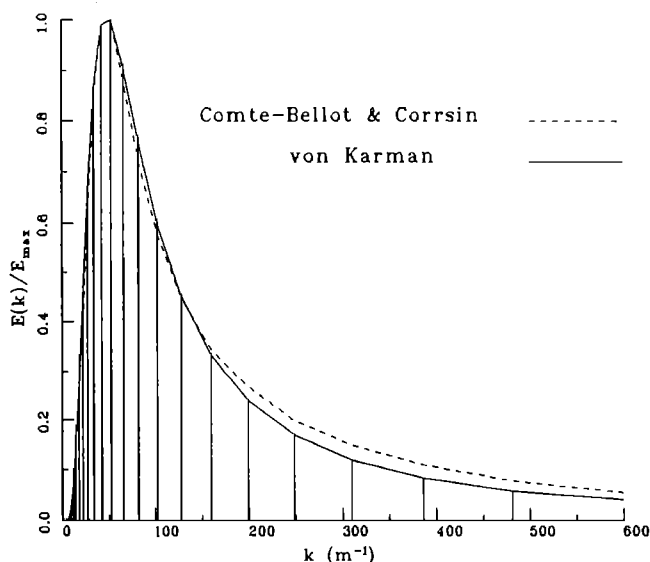
FIG. 2. Comparison of the experimental velocity spectrum of Comte–Bellot and Corrsin and the theoretical spectrum of von Karman. Vertical lines indicate spacing of Fourier modes in the simulated fields.

the integral length scale) and doubled the time to obtain them.

The spectral range over which the velocity fields were constituted was determined by the convective and refractive characteristics of acoustic ray propagation. The bandwidth of the spectrum had to include not only virtually all the energy-containing wave numbers for the convective disturbances, but also those wave numbers contributing to appreciable velocity gradients for the refractive contribution. With $\eta = 0.0001$ m in the Pao extension to our spectrum, velocity gradients are still increasing with k up to our maximum wave number. But the distance over which these gradients act, $1/k$ times the velocity gradient, is the important effect. At $k = 1000$ m^{-1} this parameter plays a diminishing refractive role. At the low end of the spectrum, we chose a minimum wave number $k_{min} = 1$ m^{-1}, corresponding to approximately 1 decade of wave numbers below the von Karman length scale.

Within this spectral range, the distribution of Fourier modes was to be selected. Three that were considered were uniform, random, and logarithmic. Randomly picked wave numbers for a given field of only 30 modes would not necessarily span the spectral bandwidth; and hence, that procedure was rejected. Of the two remaining, logarithmically spaced modes would best represent the spectral characteristics of a velocity field at low wave number. Since phase fluctuations of acoustic wave fronts are theoretically more influenced by low wave numbers (Tatarski, 1971), the logarithmic distribution was used.

The final velocity field-generation question involved whether the amplitudes of the velocity vectors corresponding to each of the wave vectors should be deterministic or random with the appropriate von Karman value or average. Although some of the earlier numerical turbulence experiments used Gaussian-distributed amplitudes (e.g., Kraichnan, 1964), current wisdom is to use amplitude deterministically prescribed by the energy spectrum. Rogallo (1981) and Rogallo and Moin (1984) suggest that simulated time-dependent flows are very sensitive to the initial conditions of the large scales and, consequently, the amplitudes of those scales are best not left to chance. Though our fields will not be evolved in time, we use the Rogallo strategy of deterministically prescribing the spectral amplitudes.

To ensure that our field-generation technique produced reasonable results, we produced an ensemble of 5000 fields corresponding to the C-BC data. (Since preliminary runs indicated that there was no measurable difference in the statistics of fields generated with a "correct" Taylor microscale of $\eta = 0.0001$ and $\eta = 0.0$, for computational efficiency we produced our ensemble with $\eta = 0.0$.) From this ensemble, and at 100 random positions within each field, we calculated the first four single-point moments for the three components of velocity and the nine components of velocity derivative. For both the velocity and its derivatives we obtained nominally zero (less than 0.02) for all the odd moments. (In grid-generated turbulent flow, the third moments of the velocity derivatives are nonzero, hence our fields were not perfect analogs. But since nonzero velocity-derivative skewness is usually attributed to the dynamics of the field, we assumed

this shortcoming to be relatively unimportant.) The second moments of velocity yielded $\langle u_1^2 \rangle = \langle u_2^2 \rangle = \langle u_3^2 \rangle = $ const. The second moments of the velocity derivatives yielded $\langle (\partial u_i / \partial x_i)^2 \rangle = 0.5 \langle (\partial u_i / \partial x_j)^2 \rangle$; and a velocity-derivative calculation of the Taylor microscale matched that in C-BC. Finally, the fourth moments all approached the value for a Gaussian pdf—3.00 (± 0.02). (In this paper, $\langle ... \rangle$ denotes ensemble averaging. But for these moment statistics, the notation also includes field averaging.) Additionally we estimated the two-point statistics

$$R_{11}(r,0,0) = \langle u_1(0,0,0) u_1(r,0,0) \rangle / \langle u_1^2 \rangle$$

and

$$R_{22}(r,0,0) = \langle u_2(0,0,0) u_2(r,0,0) \rangle / \langle u_2^2 \rangle,$$

the so-called Karman–Howarth longitudinal and lateral correlation functions, $f(r)$ and $g(r)$. These are shown in Fig. 3. Numerically integrating separately $f(r)$ and $g(r)$ with respect to r produced calculations of our fields' longitudinal and lateral integral length scales $L_f = 0.025$ m and $L_g = 0.014$ m, respectively. This compares favorably with the C-BC values of $L_f = 0.024$ m and $L_g = 0.0127$ m. Here, L_g is theoretically expected to be one-half L_f for isotropic turbulence.

With the assurance that we could asymptotically approach the statistical character of the C-BC grid-generated flow, we redefined the von Karman length scale L_0 in our field-generating scheme to be 0.09 m to model B-B's jet-generated turbulent flow with $L_f = 0.067$ m. (Theoretically, $L_0 = 1.339 L_f$ for a von Karman spectrum, i.e., with $\eta = 0.0$.) We configured our algorithm to produce $u_1' = 2$ m/s—a turbulence level bracketed by his series of experiments. And, again, we produced an ensemble of 5000 fields.
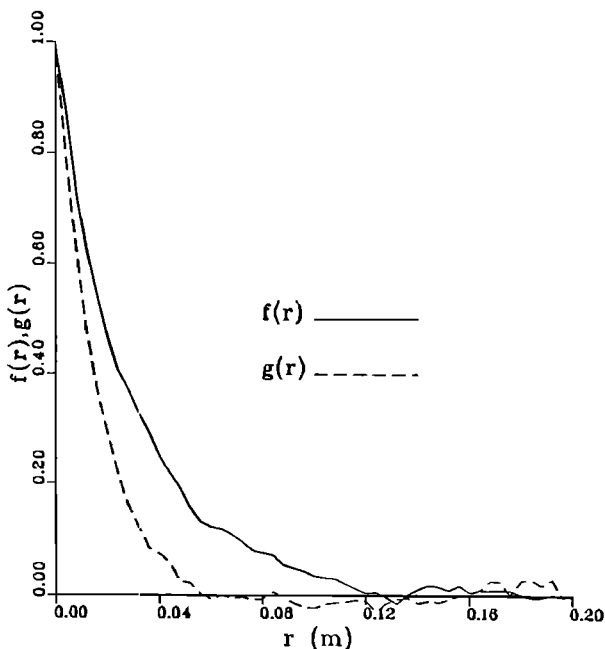
FIG. 3. Simulated longitudinal and lateral correlation functions $f(r)$ and $f(g)$, where r is the distance of separation. Results accumulated over 5000 realizations on velocity fields having a von Karman spectrum best matching the Comte-Bellot and Corrsin data.

With these fields we calculated $L_f = 0.068$ m—a value in close agreement with experiment.

II. SIMULATING THE PROPAGATION OF AN ACOUSTIC WAVE

Having described the technique to generate random velocity fields of known statistical properties, we now turn to the propagation of acoustic wave fronts through those fields.

We employ the principles of geometrical acoustics which are valid for small amplitude variations over an acoustic wavelength, a large radius of curvature of a wavefront in comparison with its wavelength, and a small wavelength in comparison with the characteristic length scale of the disturbing medium. (See, for example, Chernov, 1960). In our scheme, we assume an initial position and direction of propagation of an acoustic wave front, "tag" a point on that wave front, and follow its trajectory through the velocity field, i.e., we carry out a process known as "ray tracing."

Pierce (1981) [Eq. (8-1.10)] and Candel (1977) express the ray-tracing equations in a particularly suitable form for our application. In these developments, a parametric variable, a "wave-slowness" vector s, is introduced to describe the propagation characteristics of the tagged point on the wave front. Here, s points in the direction of propagation and has a magnitude equal to the reciprocal of the wave front's speed. Six coupled, nonlinear differential equations are required: three describing the motion of the tagged point and three describing the evolution of the slowness vector identified with that point. In this scheme the differential equations are defined exclusively in terms of the propagation field and its spatial gradients. From Pierce,

$$\frac{dx_i}{dt} = \frac{c^2 s_i}{\Omega} + u_i,$$

$$\frac{ds_i}{dt} = -\frac{\Omega}{c}\frac{\partial c}{\partial x_i} - \sum_j s_j \frac{\partial u_j}{\partial x_i}, \qquad (2)$$

where $\Omega = 1 - \mathbf{u \cdot s}$ and $c(\mathbf{x})$ and $u_i(\mathbf{x})$ are the sound-speed and velocity components of the field at the position of the tagged point on the wave front. (Although our simulations are intended to involve fields in which only velocity disturbances are present, and so the terms involving refractive gradients could be omitted, some of our experiments emulate theoretical results in which the velocity disturbances are replaced by "equivalent" scalar refractive fields.)

In this formulation we can calculate the right-hand side of the differential equations exactly at every point along a trajectory. Since our turbulent velocity fields have been modeled in terms of a fixed number of discrete Fourier velocity modes, we can obtain the spatial derivatives of the fields analytically at every point. Thus throughout an integration of a ray trajectory, there will be no accumulated error associated with the usual finite-difference approximation to these derivatives. Insofar as we integrate over long distances, this feature is critical to its success.

Our simulation procedure is straightforward. We first generate a random velocity field, i.e., select the random components of our Fourier modes. Then pick a point(s) within the field at which we presume to be on an acoustic wave front [e.g., x(0) = (0,0,0)], giving the wave front at that point a

propagation attribute by specifying a slowness vector [e.g., $s(x(0)) = \{1/[c_0 + u_1(x(0))],0,0\}$]. Then we numerically follow the trajectory of that point and the evolution of the slowness vector over time with a fourth-order Runge–Kutta integration scheme.

Computations are carried out in double precision with an integration time step of $\Delta t = 1/(c_0 k_{max})$—the longest step for which results duplicate those obtained from integrations of half that step size. In our simulations we assume the transit time of an acoustic wave is short compared to any time scale in the velocity field and, hence, we follow a trajectory within a "frozen" field; i.e., there is no time evolution of the field during our integrations.

Over ensembles of 250 to 1000 such individual integrations, each using a different random velocity field, we record time of propagation at various distances R from the "source"; then we accumulate statistics. In most cases, choosing the number of realizations to be 1000 effected stable acoustic time-variance estimates and practical execution times for the computer runs. (The 1000-realization experiments require approximately 20 h of MicroVax II CPU time.)

Except for our experiments in "one-dimensional" propagation, there is no *a priori* way to predict the point at which a ray will have propagated a distance R. So our definition of a propagation distance R was the spherical shell of positions $\sqrt{x_1^2 + x_2^2 + x_3^2} = R$.

III. NUMERICAL EXPERIMENTS

A. The Chernov approximation—Straight-line ray propagation

Chernov approximates the transit time for acoustic rays by assuming that deviations from a straight trajectory are negligible and produces the transit time to a distance R:

$$t = \frac{1}{c_0} \int_0^R n(x_1,x_2,x_3)dx_1, \qquad (3)$$

where $n(x_1,x_2,x_3)$ is the index of refraction of the medium along the ray. For an inhomogeneous medium consisting only of velocity fluctuations, $n = 1 + \mu$ with $\mu \approx -u_1/c_0$. The transit-time variance can then be expressed when $R \gg L_f$ by

$$\langle t'^2 \rangle = \frac{2\langle \mu^2 \rangle R}{c_0^2} \int_0^\infty N(x_1,x_2,x_3)dx_1, \qquad (4)$$

where $N(x_1,x_2,x_3)$ is the normalized correlation function of μ. Since the departures of ray trajectories from $x_2 = x_3 = 0$ are assumed to be small, Chernov reduces the integrand to $N(x_1,0,0)$ [Chernov, 1960, Eq. (68)]. For an isotropic field consisting only of velocity fluctuations

$$\int_0^\infty N(x_1,0,0)dx_1$$

is just the integral length scale L_f. Thus (4) can be rewritten as

$$\langle t'^2 \rangle = (2\langle u_1^2 \rangle R /c_0^4)L_f. \qquad (5)$$

[We remark that the same linear dependence of $\langle t'^2 \rangle$ with R is obtained by using a smooth-perturbation analysis on the wave equation in the limits of both very large and very small values of the wave parameter $D = 4R/(\kappa_0 d^2)$ (Tatarski 1971). R is the transit distance, $d \approx L_f$ is the mean size of the inhomogeneities of the field, and κ_0 is the acoustic wave number in the medium at rest.]

To establish that our technique for studying acoustic propagation was viable, we reduced our governing ray equations to ignore all nonaxial components and, of course, density-inhomogeneity terms, since our fields were constant density. Thus we could simulate the Chernov approach. In this case our equations reduced to the two equations

$$\frac{dx_1}{dt} = \frac{c_0^2 s_1}{\Omega} + u_1,$$

$$\frac{ds_1}{dt} = -s_1 \frac{\partial u_1}{\partial x_1}, \qquad (6)$$

with $\Omega = 1 - u_1 s_1$. Over an ensemble of 1000 realizations we simulated unidirectional ray propagation and generated the variance of arrival times at different distances from the origin. In Fig. 4 we present the outcome. Propagation distance is given in terms of the integral length scale L_f. Time variance is normalized by the Chernov solution evaluated at the distance $R = 40L_f$. Recall that the parameters of the field are $L_f = 0.067$ m and $u_1' = 2$ m/s.

The Chernov solution, assumed to be valid for large distances of propagation, predicts a linear growth of time-(phase) variance with distance of propagation. Clearly our simulations confirm that result.

Near the origin, the integral in (4), which becomes L_f at larger distances, integrates to a lesser value. Consequently, at short distances, travel-time variance falls below the asymptotic result. In all the experiments that follow, this "dip" is apparent.
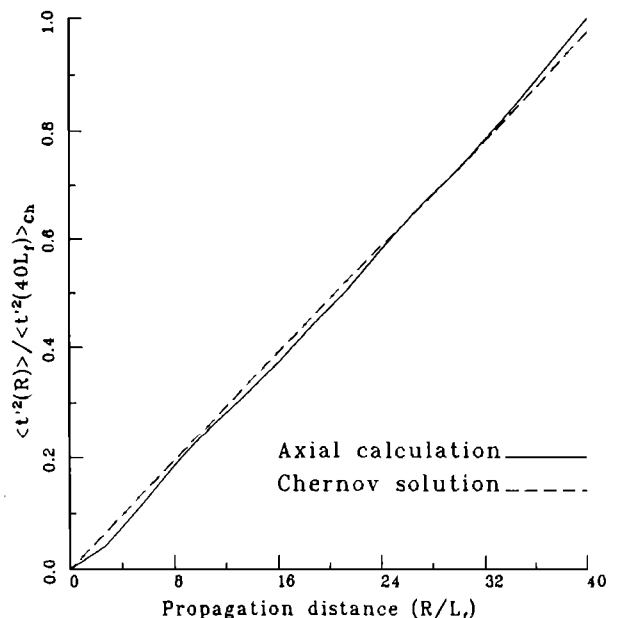
FIG. 4. Arrival time variance of simulated acoustic rays constrained to axial propagation. Results accumulated over 1000 realizations and normalized with respect to the Chernov solution $\langle t'^2 \rangle_{ch}$ at a distance of $40L_f$. The Chernov solution is plotted for comparison.

B. Ray-trace simulations

With the same field characteristics as above, we carried out a second set of trajectory calculations—this time using the full ray-trace equations [Eq. (2)]. That is, in contrast to the simulation above, we retained the nonaxial velocity terms and reinstated the equations that provide for lateral excursions of the ray trajectories.

Figure 5 shows the results, again scaled in distance of propagation by L_f and normalized in time variance by the Chernov result at $R = 40L_f$. It is obvious that with full ray tracing, time variance is not proportional to propagation distance. In fact, if a power law were to be imposed on the result, the best fit over the interval $R = 0$ to $R = 20L_f$ is $\langle t'^2 \rangle \sim R^{1.6}$. This outcome is unexpected, but, as we shall see, not inconsistent with the numerical experiments that follow.

C. Stochastic Helmholtz solutions

A description for sound propagation through a turbulent field is approximated by the so-called stochastic Helmholtz equation:

$$[\nabla^2 + \kappa_0^2 n^2)]P(x) = 0, \tag{7}$$

where $\kappa_0 =$ acoustic wave number in the medium at rest and $P =$ wave pressure. For forward scattering the refraction index n can be described in terms of the "perturbation" index ϵ as $n^2 = c_0^2/c^2 = 1 + \epsilon$, where $\epsilon = -2u_1/c_0 - \tau'/T$. (The term τ'/T is the contribution due to temperature inhomogeneities and is neglected in the present study.) Several approximations are required for this explicit form (Tatarski, 1971; Candel, 1979; Neubert, 1970; Neubert and Lumley, 1970).
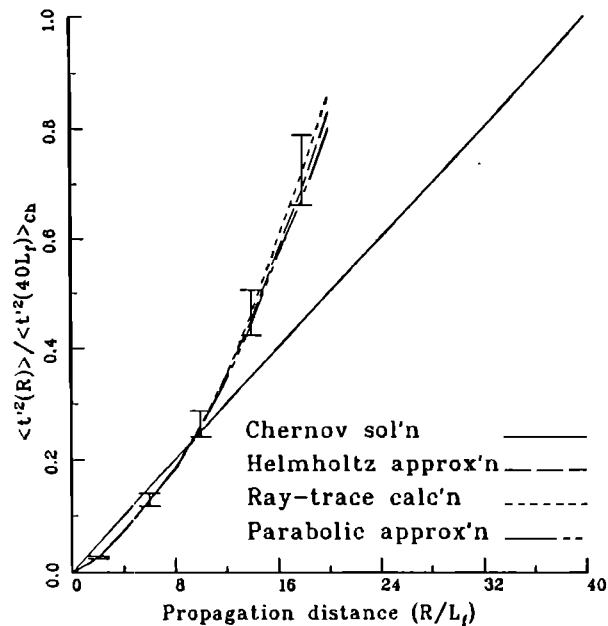
FIG. 5. Arrival time variances in simulations using three different ray-trace approximations. Results accumulated over 1000 realizations and normalized with respect to the Chernov solution $\langle t'^2 \rangle_{Ch}$ at a distance of $40L_f$. A 0.95 confidence band is indicated for the ray-trace calculation. The Chernov solution is plotted for comparison.

Figure axes: vertical $\langle t'^2(R) \rangle / \langle t'^2(40L_f) \rangle_{Ch}$ from 0.0 to 1.0; horizontal Propagation distance (R/L_f) from 0 to 40.

Legend:
Chernov sol'n ———
Helmholtz approx'n — — —
Ray-trace calc'n - - - - - -
Parabolic approx'n —— ··

Note that the influence of the disturbances of the field is limited only to those in the axial direction, and velocity disturbances look like scalar rather than vector disturbances. We can simulate this approximation by treating our velocity fluctuations as fluctuations in the refractive index, and send hypothetical rays through an equivalent inhomogeneous scalar field, rather than through our actual velocity field.

Under these conditions $\Omega = 1$ and our ray equations for "scalar" inhomogeneities become

$$\frac{dx_i}{dt} = \frac{c_0^2}{(1 - 2u_1/c_0)} s_i,$$

$$\frac{ds_i}{dt} = -\frac{1}{c_0(1 - 2u_1/c_0)} \frac{\partial u_1}{\partial x_i}. \tag{8}$$

A first-order approximation of the relation $n^2 = 1 - 2u_1/c_0$ gives $c = c_0(1 + u_1/c_0)$. This provides an illustration of the difference between the exact ray and the "Helmholtz" ray. In the former case, the propagation velocity is given by a vectorial addition of $c_0 s/|s|$ and u, where $s/|s|$ is the unit normal to the wave front. In the latter, the propagating velocity is approached by $(c_0 + u_1)s/|s|$. Because of the small magnitude of u in comparison with c_0, the angular difference between the two methods is very small and the results of the two approaches should be in close agreement.

With these equations, we again carried out an ensemble of ray-tracing experiments and produced the time-variance results included in Fig. 5. Time variance is still not linearly related to travel distance, and is in fact in full agreement with the results of the complete ray-tracing experiments.

D. A parabolic approximation solution

A widely used approximation to the Helmholtz equation in acoustics (and optics) is the parabolic approximation. By assuming that acoustic propagation is primarily along a principal direction, say, the x_1 axis, and the acoustic pressure takes the form $P = \exp(i\kappa_0 x_1) \Psi(x)$ in the Helmholtz equation, the second derivative of Ψ with respect to x_1 is negligible compared to the first derivative, and the result takes a parabolic form. (See the discussions by Tappert, 1977 and Candel, 1979). Then (7) reduces to

$$2i\kappa_0 \frac{\partial \Psi}{\partial x_1} + \frac{\partial^2 \Psi}{\partial x_2^2} + \frac{\partial^2 \Psi}{\partial x_3^2} + \kappa_0^2 (n^2 - 1)\Psi = 0. \tag{9}$$

If one gives to Ψ the form $\Psi \sim e^{i\kappa_0[S(x) - x_1]}$ (S being related to the slowness vector s by $\nabla S = c_0 s$), the eikonal equation can be expressed in terms of the components $Q_i = \nabla_i S$:

$$2Q_1 + Q_2^2 + Q_3^2 - n^2 - 1 = 0. \tag{10}$$

Thus the eikonal relation is of the form $H(Q, S, x) = 0$. This represents a nonlinear, first-order equation soluble by the method of characteristics. Following Whitham [(1974), Eqs. (2.82–2.88)] we deduce the ray-tracing equations in terms of the auxiliary variable σ. (Integration along a characteristic is not, in general, orthogonal to the acoustic wave front in this approximation. Thus to obtain propagation time, the auxiliary variable σ and an additional equation is required.) We obtain

$$\frac{dx_1}{d\sigma} = c_0,$$

$$\frac{dx_2}{d\sigma} = c_0 Q_2,$$

$$\frac{dx_3}{d\sigma} = c_0 Q_3, \qquad (11)$$

$$\frac{dQ_i}{d\sigma} = c_0 n \frac{\partial n}{\partial x_i},$$

$$\frac{dt}{d\sigma} = Q_1 + Q_2^2 + Q_3^2 = n^2 + 1 - Q_1.$$

The last equation concerning the propagation time t is obtained by making use of $S = c_0 t$. The initial conditions, corresponding to a horizontal ray are $Q_2 = Q_3 = 0$, and $Q_1 = 0.5(n^2 + 1)$.

With these equations, an ensemble of rays was numerically followed and the final curve on Fig. 5 was produced, a result again agreeing with the complete ray-trace curve.

E. Experimental results (laboratory)

The difficulty of obtaining laboratory measurements of phase or time-of-flight variance is indicated by the dearth of data. Other than Ho and Kovasznay (1974) who made such measurements across an airjet (but over an extremely short propagation distance), only the experiments of B-B are published. In his experiments, B-B generated an approximately plane acoustic wave with a pistonlike sound source and aimed it across jet-generated air flows having turbulence levels $u_1' = 2.4$ m/s and 1.1 m/s. At a distance of 1 m from the nozzle, he measured acoustic phase variance at four acoustic frequencies: 31.25, 41.66, 50.00, and 83.33 kHz.

In a final group of numerical experiments, we carried out our ray-tracing technique to simulate these laboratory ones; i.e., we used fields having the same integral length scale and turbulence levels. The results, along with the Chernov approximation and B-B's data points are plotted in Fig. 6. Laboratory phase variances have been converted to time variances by the relation $\omega t = \Phi$, a relation justified by the quasilinear dependence of $\sqrt{\overline{\Phi^2}}$ vs ω found in the experiments (relative error $< 5\%$). B-B's measurements at his lower turbulence level are very close to both the Chernov prediction and the numerical simulation. At his higher turbulence level, the measurements follow neither. However, they are in qualitative agreement with the nonlinear form predicted by the ray-trace simulations.

That B-B's experiments are applicable to our ray-trace simulations can be evaluated using a Λ–Φ diagram devised by Flatté et al. (1979). In this scheme acoustic conditions can be categorized into "saturated," "partially saturated," and "unsaturated" zones based on $\Phi = 2L_f k_0^2 R \langle \mu^2 \rangle^{1/2}$, the rms value expected for phase variance and $\Lambda = R / (L_f^2 k_0)$, a diffraction parameter. Figure 7 places B-B's five cases on such a Λ–Φ diagram, with zone boundaries having been calculated for a Kolmogorov spectrum $E(k) \sim k^{-5/3}$. Here, we show that most of the experimental data are within the geometric acoustics (unsaturated) regime. Only the case
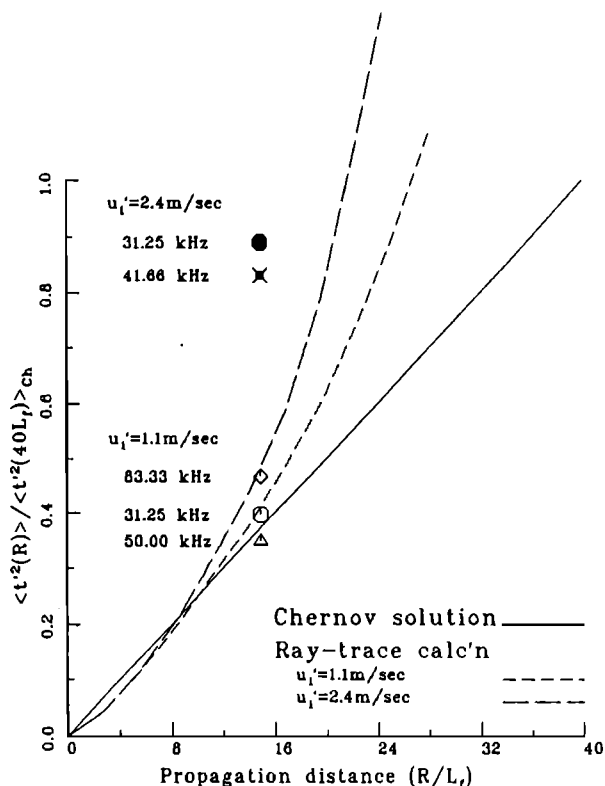
FIG. 6. Arrival time variances of numerical experiments compared with the laboratory experiments of Blanc-Benon. Results accumulated over 1000 realizations and normalized with respect to the Chernov solution $\langle t'^2 \rangle_{ch}$ at a distance of $40L_f$. The Chernov solution is plotted for comparison.

$u' = 2.4$ m/s, $f = 41.66$ kHz reaches the partially saturated region.

We should remark that these zone boundaries are somewhat qualitative. And with B-B's experiments occurring close to the region of partial saturation, his results may be slightly contaminated by effects not covered by weak fluctuation theory. Thus comparisons must be made with caution.

IV. DISCUSSION

Based on the assumption that acoustic waves passing through a turbulent medium depart little from straight-line propagation, current thought—i.e., the Chernov solution—is that acoustic phase variance is proportional to propagation distance. In the numerical experiments just described, that assumption is typically not met. Only in the case where we force a ray to follow an axial trajectory do we produce the linear result. In all of the other simulations—the ones in which we allow for three-dimensional motion—we produce phase variances that have not only linear components, but higher-order terms as well.

There is a work that seems to predict this result. Katz (1963) analyzed ray propagation in a 2-D scalar inhomogeneous medium by carrying out a small parameter expansion of the ray-trace equations and produced an expression for travel-distance variance as a function of time. His analysis produced both a linear and a third-order term. But the result is only indirectly applicable to our investigation because we consider the converse problem—time variance as a
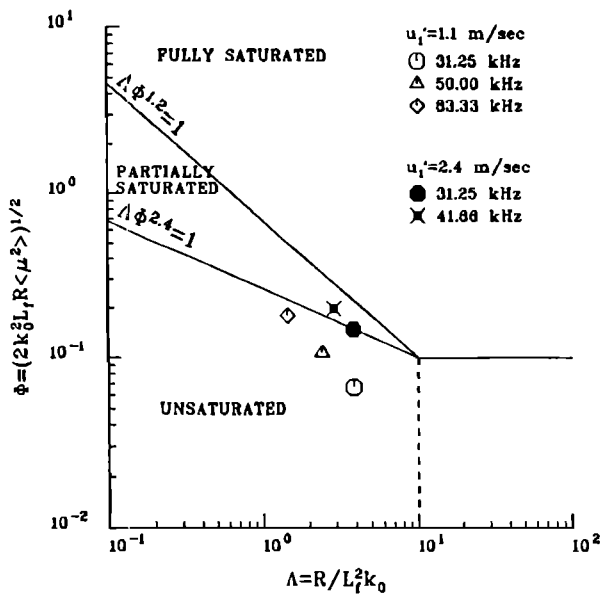
FIG. 7. Blanc-Benon experimental conditions in terms of a Flatté phase variance–diffraction (Λ–Φ) diagram. Zone boundaries are calculated for a Kolmogorov spectrum $E(k) \sim k^{-5/3}$.

function of distance—and there is no obvious way to invert his expression.

The Chernov solution, having been derived for a source–receiver problem, is inherently different from our PID simulation. Does this difference in approach account for the apparent difference in predicted phase-variance behavior?

To explore this possibility, we conducted a final set of numerical experiments in which our simulation technique was used to calculate the phase variance of both source–receiver rays (eigenrays) and PID rays. In the eigenray experiments, for each realization of a velocity field the trajectories of a large number of rays were calculated, each ray starting with a different initial direction. Only those rays that passed through a preassigned end point (receiver) were used in calculating transit-time statistics.

Since computing eigenrays in three-dimensional fields would have been too formidable a task, we restricted this set of experiments to two dimensions. The velocity fields were based on a Gaussian correlation function $f(r) \sim \exp(-r^2/L^2)$ which yields a 2-D kinetic-energy spectrum $E(k) = \left[\overline{u_1^2} k^3 L^4/8 \right] \exp(-k^2 L^2/4)$. This form, very suitable for numerical computations because of its limited wave-number range, has been previously used to analyze the focusing effect of waves by inhomogeneous scalar fields (e.g., Zwillinger and White, 1985). $L = 0.1$ m was used to yield an integral length scale $L_f = L\sqrt{\pi}/2$. Fields were generated using 50 randomly oriented velocity wave vectors, uniformly spaced in wave number between $k_{min} = 1$ m^{-1} and $k_{max} = 100$ m^{-1}.

Over an ensemble of 250 of these simplified fields, the two ray-trace experiments were performed. First, the usual one: Rays were assigned initial directions along the x_1 axis and tracked until they reached a prescribed distance R. Second, the source–receiver simulation: Here, we looked for an initial ray direction such that the ray would pass through the x_1 axis at a distance R. These eigenrays were selected by following a fan of 200 rays having initial directions over the range ± 10 deg in increments of 0.1 deg, and then interpolating linearly between adjacent rays to find a new launching angle that would enable that ray to cross the receiver location at the given distance R. The transit time of this new ray was then recorded. In this way most, if not all, eigenrays were accounted for.

Note that although both experiments were carried out over an ensemble of 250 fields, the eigenray experiment produced more than 250 contributions for large source–receiver separations. The additional contributions result from having more than one eigenray per field, hence the occurrence of caustics. Table I gives the number of eigenrays as a function of the normalized distance of propagation R/L_f.

Clearly, there is one eigenray per realization up to $R/L_f \simeq 15$, so that up to this distance caustics apparently do not occur. Beyond that, however, the number of additional rays increases rapidly with R/L_f.

Figure 8 indicates travel-time variances for the two experiments, again superposed on the Chernov prediction. A principal observation is that the two sets of variances are similar—both showing trends that appear to be initially linear, and finally nonlinear. Further, in comparing these curves with Figs. 5 and 6, our 3-D results, one observes no qualitative difference.

The approximately linear region for the eigenrays in Fig. 8, i.e., for $R/L_f < 20$, is a region before significant caustics. But any linear fit falls somewhat below the Chernov estimate. Overall, it appears that simulations of the source–receiver problem are comparable to the experiments with PID rays. Whether there is any difference in functional form of travel-time variance before and after the onset of caustics in the eigenray experiment is open to question.

We can synthesize our collective results in a particularly informative way—one that decomposes the travel-time variance into linear and nonlinear contributions. For each of our

TABLE I. Number of eigenrays as a function of the normalized distance of propagation R/L_j.

R/L_j	Number of eigenrays	Additional rays
2.25	250	0
4.51	250	0
6.77	250	0
9.02	250	0
11.28	250	0
13.54	250	0
15.79	252	2
18.05	254	4
20.31	256	6
22.56	260	10
24.82	276	26
27.08	283	33
29.33	296	46
31.59	314	64
33.85	337	87
36.10	355	105
38.36	373	123
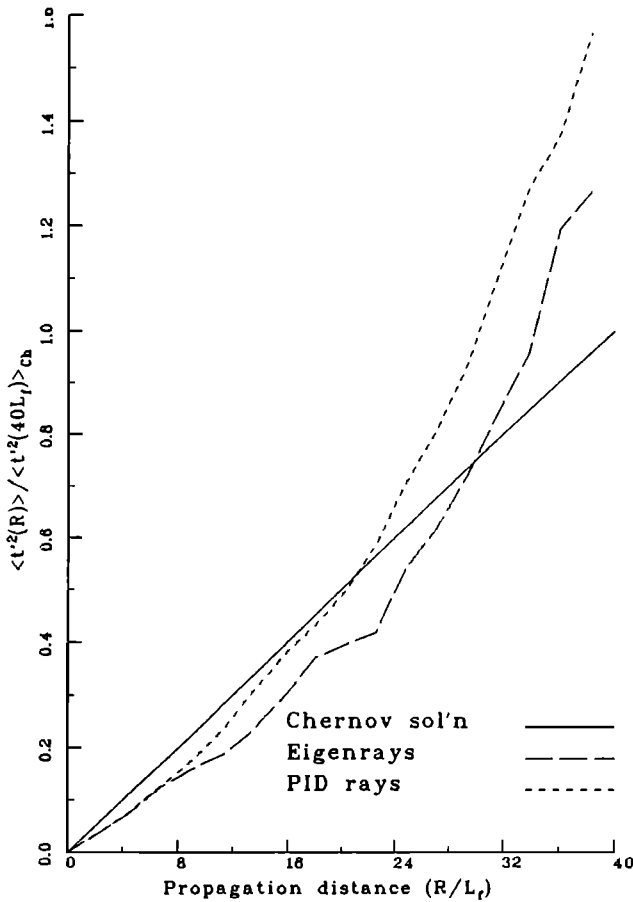
FIG. 8. A comparison of arrival-time variances for propagation through two-dimensional Gaussian fields (250 realizations). Eigenrays begin at $x = (0,0)$ with directions such that each propagates past the point $x = (R,0)$, i.e., the source–receiver problem. Preassigned-initial-direction (PID) rays begin at $x = (0,0)$ with direction x_1 and propagate to $|x| = R$. Results are normalized to the Chernov calculation at a distance of $40L_f$.

experiments we fit our data to a two-term function of the following normalized form:

$$\frac{\langle t'^2(R/L_f)\rangle}{2\langle u_1^2\rangle L_f^2/c_0^4} = a_1\left(\frac{R}{L_f}\right) + a_p\left(\frac{R}{L_f}\right)^p. \qquad (12)$$

We force the variance to be zero at the origin; and by normalizing $\langle t'^2\rangle$ as indicated—the Chernov prediction at $R/L_f = 1$, we expect a Chernov variance dependency to yield $a_1 = 1.0$ and $a_p = 0.0$. Table II reflects fitting the above equation to our complete set of experiments.

Two features are evident. First, the coefficients of the linear terms are noticeably less than the Chernov value. Only when the simulation is limited to axial trajectories does $a_1 \approx 1$ (and $a_p \approx 0$). Second, each nonaxial simulation has an obvious nonlinear component.

To characterize this nonlinearity further, we computed for each simulation the distance at which the nonlinear component comprised 20% of the total variance. The results are clustered by dimension: They lie between 3 and 13 L_f for the 3-D simulations, and between 15 and 23 L_f for the 2-D ones—the 23 L_f value being calculated for the eigenrays. As we noted above in commenting on Fig. 8, 23 L_f is the approximate distance of the onset of significant caustics.

TABLE II. Coefficients for polynomial approximation to phase variance [Eq. (12)].

Simulation	Fig. no.	a_1	a_p	p
Ray-trace (3-D)	5	0.510	$4.28e - 02$	2.1
Helmholtz (3-D)	5	0.479	$4.64e - 02$	2.1
Parabolic (3-D)	5	0.467	$5.71e - 02$	2.0
B-B 1.1 m/s (3-D)	6	0.748	$4.82e - 03$	2.5
B-B 2.4 m/s (3-D)	6	0.765	$2.20e - 03$	3.0
PID rays (2-D)	8	0.721	$1.29e - 03$	2.8
Eigenrays (2-D)	8	0.677	$2.48e - 05$	3.8
Axial rays (1-D)	4	0.983	$- 8.74e - 09$	3.6

If caustics are a contributing factor, there is a possible explanation for the 20% distances being smaller in the 3-D simulations: The shape of the 2-D Gaussian spectrum is different from that of the 3-D von Karman spectrum. In the 3-D case, the von Karman spectrum has a relatively longer "tail" toward high wave number. At least in scalar inhomogeneous fields, the relevant parameter for the occurrence and spacing of caustics is the fourth derivative of the two-point spatial correlation function (Kulkarny and White, 1982). And this parameter is significantly influenced by a long spectral tail.

The 2-D simulations allowing us to compare travel-time variances between eigenrays and PID rays also give us the opportunity to compare mean travel times. We have observed that there is little qualitative difference between source–receiver and PID experiments with respect to travel-time variance. However, these conclusions do not apply to travel-time means. Observe Fig. 9, a plot of average travel times for our experiments in two dimensions. Remarkably, the PID rays are progressively retarded with respect to acoustic travel time in an undisturbed medium; whereas the
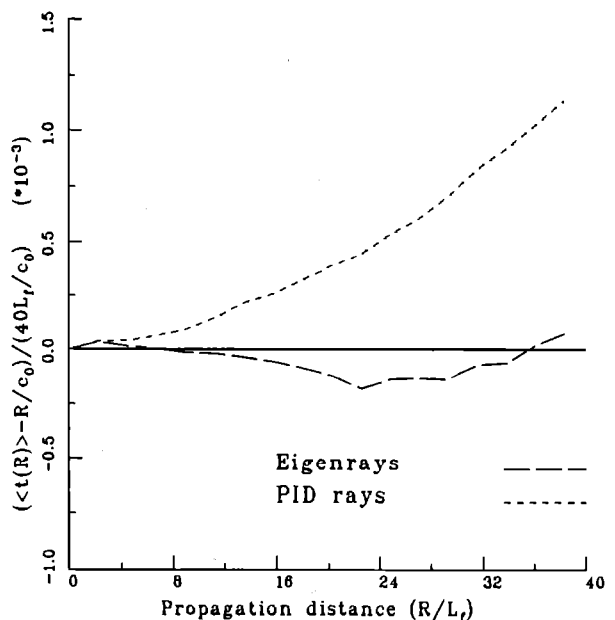
FIG. 9. A comparison of mean arrival times for eigenray propagation and preassigned-initial-direction (PID) ray propagation through two-dimensional Gaussian fields (250 realizations). Results are presented as differences from a transit time through a homogeneous medium R/c_0 and normalized in terms of that travel time for a distance $40L_f$.

eigenrays are initially advanced. Perhaps not coincidentally, the mean travel time of eigenrays begins to increase beyond $R/L_f \approx 20$—the onset of significant caustics. Note that the PID ray averages exhibit no change in trend.

The eigenray results are anticipated. In a source–receiver thought experiment, Codona et al. (1985), invoked Fermat's principle to show that the mean time for a pulse to travel a distance R in a turbulent field (modeled as a continuum of phase screens) must be shorter than R/c_0, the time to travel through a homogeneous field. But this result is obtained in the range of no caustics. They show further that, beyond that range, one should expect travel times to increase—eventually above the homogeneous field travel time.

The PID ray travel-time averages, however different, have also been predicted. Katz (1963), in his 2-D analysis, generates an expression that not only indicates ray retardation, but also shows quantitative agreement with our 2-D results. [Here, we are able to invert his expression for $\bar{R}(t)$ to $\bar{t}(R)$.] He identifies two retarding terms: one due to increased path length, the other due to the predisposition of rays to turn toward regions of slower sound speed. See also Keller (1962) for a 3-D analysis of ray tracing and Wenzel and Keller (1971) for an approach based on the wave equation.

To complete our discussion, we illustrate with Fig. 10 the relative magnitudes of travel-time retardation and variance for our 3-D ray-trace experiment and for our 1-D axial experiment. Here, we plot the distribution of arrival times over 1000 realizations for several propagation distances. The small descending tics mark the undisturbed arrival times $t(R) = R/c_0$. In the axial case (where $R = x_1$), the distributions are symmetric with means equal to the undisturbed arrival times. In the 3-D case, the distributions are asymmetric with mean values progressively larger than the undisturbed arrival times. It is noteworthy that in this latter case the travel-time variation is significantly larger than its mean retardation.

In summary, we offer a list of tentative conclusions:

(1) Travel-time variance must be expressed as a function of propagation distance which includes both linear and higher-order terms. This result is found in the following situations: (a) preassigned initial direction ray propagation in two and three dimensions; (b) source–receiver propagation (eigenray) in two dimensions.

(2) The linear term in the relation between travel-time variance and distance equals the Chernov value only in 1 D.

(3) The Helmholtz and parabolic approximations are equivalent to the full ray-trace equations with respect to travel-time variance.

(4) Ray retardation is found in preassigned initial direction ray propagation in two and three dimensions.

(5) Ray advancement is found in 2-D eigenray propagation prior to the occurrence of caustics.

(6) Ray retardation is found in 2-D eigenray propagation after the occurrence of caustics.

V. CONCLUSION

In this work we have introduced a unique approach to studying acoustic propagation through inhomogeneous me-
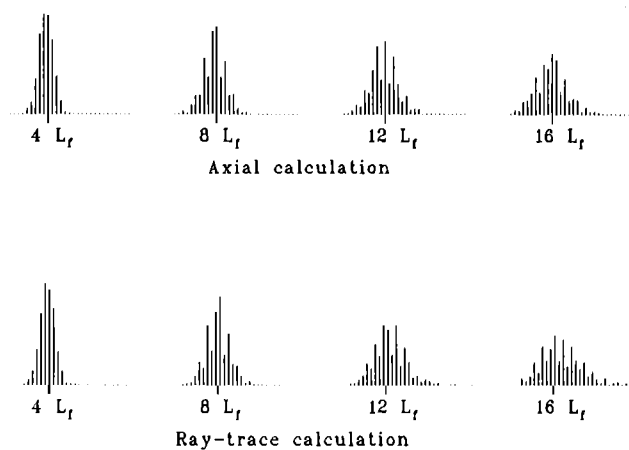
FIG. 10. Distribution of arrival times of acoustic rays for axial and full ray-trace propagation over 1000 realizations. Propagation distances are given in units of L_f. The descending tic marks denote arrival times for a constant acoustic speed of c_0.

dia. By characterizing a field in terms of a collection of Fourier modes, we have provided a means by which the acoustic ray-trace equations can be evaluated analytically at every point along a path. Thus we can perform accurate numerical simulations that are analogous to laboratory experiments. Unlike laboratory experiments, these simulations can map out the complete history of an acoustic wave. And, unlike laboratory experiments, these simulations can be performed with exact prescriptions of field properties and acoustic wave-front characteristics.

The technique can be used in a variety of applications. Currently we are extending the approach to study the occurrence of caustics in velocity-inhomogeneous fields having different spectral characteristics, and to study acoustic dispersion in density-inhomogeneous fields. Further, by selecting a small circle of "tagged" points to delineate the perimeter of a hypothetical ray tube and following these points' propagation, one could infer acoustic intensity variability as well.

Finally, we have seen that other approaches providing acoustic pressure repartitions, such as the parabolic approximation, can also be adapted to simulations involving random fields. Our method could be particularly useful for predicting acoustic intensity fluctuations in unsaturated or saturated conditions.

Blanc-Benon, P. (1981). "Effet d'une turbulence cinématique sur la propagation des ondes acoustiques," Thèse Docteur-Ingénieur, Ecole Centrale de Lyon, No. 81-02.

Blanc-Benon P., Chaize, S., and Juvé, D. (1986). "Coherence aspects of acoustic wave transmission through a medium with temperature fluctuation," Aero- and Hydro-acoustics IUTAM Symposium LYON, 1986 (Springer-Verlag, Berlin), pp. 217–226.

Candel, S. (1977). "Numerical solution of conservation equations arising in linear wave theory: Application to aeroacoustics," J. Fluid Mech. 83, 465–493.

Candel, S. (**1979**). "Numerical solutions of wave scattering problems in the parabolic approximation," J. Fluid Mech. **90**, 465–507.

Chernov, L. (**1960**). *Wave Propagation in a Random Medium* (McGraw-Hill, New York).

Codona, J. L., Creamer, D., Flatté, S., Frehlich, R., and Henyey, F. (**1985**). "Average arrival time of wave pulses through continuous random media," Phys. Rev. Lett. **55**, 9–12.

Comte-Bellot, G., and Corrsin, S. (**1971**). "Simple Eulerian time correlation of full- and narrow-band velocity signals in grid-generated, 'isotropic' turbulence," J. Fluid Mech. **48**, 273–337.

Dashen, R. (**1979**). "Path integrals for waves in random media," J. Math. Phys. **20**, 894–920.

Fishman, L., and McCoy, J. L. (**1984**). "Derivation and application of extended parabolic wave theories," J. Math. Phys. **25**, 285–308, Pts. 1 and 2.

Flatté, S. M. (Ed.) (**1979**). *Sound Transmission through a Fluctuating Ocean* (Cambridge U.P., Cambridge).

Flatté, S. M. (**1983**). "Wave propagation through random media: Contributions from ocean acoustics," Proc. IEEE **71**, 1267–1293.

Hinze, J. O. (**1959**). *Turbulence* (McGraw-Hill, New York).

Ho, C. M., and Kovasznay, L. S. G. (**1974**). "Modulation of an acoustic wave by turbulent shear flow," U. S. Air Force Office of Scient. Res., Interim Tech. Rep., F44-620-69-C-0023.

Ishimaru, A. (**1978**). *Wave Propagation and Scattering in Random Media* (Academic, New York), Vols. 1 and 2.

Karweit, M., Blanc-Benon, P., Juvé, D., and Comte-Bellot, G. (**1988**). "Simulation of the propagation of an acoustic wave through a turbulent velocity field," Proceedings of the 17th International Union of Theor. and Appl. Mech., Grenoble, 21–27 August 1988.

Katz, E. J. (**1963**). "A ray theory for wave propagation in a non-uniform medium," J. Fluid Mech. **16**, 343–356.

Kraichnan, R. H. (**1964**). "Decay of isotropic turbulence in the direct-interaction approximation," Phys. Fluids **7**, 1030–1048.

Keller, J. B. (**1962**). "Wave propagation in random media," Proc. Symposium Appl. Math. **13**, Am. Math. Soc., Providence, RI, 227–246.

Kulkarny, V. A., and White, B. S. (**1982**). "Focusing of waves in turbulent inhomogeneous media," Phys. Fluids **25**, 1770–1784.

Neubert, J. (**1970**). "Asymptotic solution of the stochastic Helmholtz equation for turbulent water," J. Acoust. Soc. Am. **48**(5) (Pt. 2), 1203–1211.

Neubert, J., and Lumley, J. (**1970**). "Derivation of the stochastic Helmholtz equation for sound propagation in a turbulent field," J. Acoust. Soc. Am. **48** (Pt. 2), 1212–1218.

Pao, Y. H. (**1965**). "Structure of turbulent velocity and scalar fields at large wavenumbers," Phys. Fluids **8**, 1063–1075.

Pao, Y. H. (**1968**). "Transfer of turbulent energy and scalar quantities at large wavenumbers," Phys. Fluids **11**, 1371–1372.

Pierce, A. D. (**1981**). *Acoustics: An Introduction to Its Physical Principles and Applications* (McGraw-Hill, New York).

Rogallo, R. S. (**1981**). "Numerical experiments in homogeneous turbulence," NASA Tech. Mem. 81315, September 1981.

Rogallo, R. S., and Moin, P. (**1984**). "Numerical simulation of turbulent flows," Ann. Rev. Fluid Mech. **16**, 99–137.

Tappert, F. D. (**1977**). "The parabolic approximation method," in *Wave Propagation and Underwater Acoustics*, edited by J. B. Keller and J. S. Papadakis (Springer-Verlag, Berlin), Lecture Notes in Physics, 70.

Tatarski, V. I. (**1971**). *The Effects of the Turbulent Atmosphere on Wave Propagation* (I. P. S. T. Keter Press, Jerusalem).

Tatarski, V. I., and Zavorotnyi, V. U. (**1980**). "Strong fluctuations in light propagation in a randomly inhomogeneous medium," in *Progress in Optics*, edited by E. Wolf (North-Holland, New York), Vol. 18, Chap. 3.

Uscinski, B. J. (**1985**). "Analytical solution of the fourth-moment equation and interpretation as a set of phase screens," J. Opt. Soc. Am. A **2**, 2077–2091.

Wenzel, A. R., and Keller, J. B. (**1971**). "Propagation of acoustic waves in a turbulent medium," J. Opt. Soc. Am. **50**, 911–920.

Whitham, G. B. (**1974**). *Linear and Nonlinear Waves* (Wiley, New York).

Whitman, G. G., and Beran, M. J. (**1985**). "Two-scale solution for atmospheric scintillation," J. Opt. Soc. Am. A **2**, 2133–2143.

Zwillinger, D. I., and White, B. S. (**1985**). "Propagation of initially plane waves in the region of random caustics," Wave Motion **7**, 207–227.